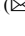






Reduction of Hot Cracks During Electron Beam Welding of Alloy-247 LC

Aleksej Senger¹ , Torsten Jokisch², Simon Olschok¹ , and Uwe Reisgen¹ 

¹ Welding and Joining Institute, RWTH Aachen University, Pontstr. 49, 52062 Aachen, Germany
senger@isf.rwth-aachen.de

² Gas and Power, Siemens AG, Nonnendamm 55, 13629 Berlin, Germany

Abstract. Alloy-247 LC belongs to the group of precipitation hardening materials and is characterized by good creep resistance at higher temperatures. Although the material offers good cast workability, the weldability of the material is very limited due to its high crack tendency. This paper identifies and optimizes electron beam welding parameters with regard to hot crack reduction when welding conventionally cast components. The crack evaluation is carried out using scanning electron microscopy and light microscopy of the upper beads and the cross sections. In order to statistically verify the results, crack identification was carried out by micro-CT measurements. A welding speed dependent dendrite arm distance measurement additionally supports the crack investigation. Furthermore, a crack-optimized welding parameter was successfully transferred to a dissimilar joint weld (conventionally solidified to directionally solidified) and the potential for welding the high-performance material Alloy-247 LC with the electron beam was demonstrated by creep tests.

Keywords: Electron beam welding · Nickel-based alloy · Alloy-247 LC · Dendrite · Hot crack · Creep test

1 Introduction

The improvements in the efficiency of gas turbines are achieved by various combinations of technological measures. These include improved cooling, development of thermal insulation layers, aerodynamic optimization of the blades, reduction of losses and the further development of materials with better high-temperature characteristics [1]. The last-named has experienced an enormous development in metallurgy over the last decades. The specific mechanical and chemical properties have been improved with increasing quantities of different alloying elements. In addition, the casting processing of the superalloy has been expanded. With the innovative alloys and the possibility of directional solidification (DS) and single crystalline solidification (SX), the efficiency and lifetime of turbine materials have been further optimized [2–4]. Alloy 247 LC is a chemically modified superalloy specially developed for directional solidified blades and guide vanes. This enables the production of complex, core-containing, thin-walled blades. From an economic point of view, a repair of the guide vanes is opportune [5]. A

hybrid design of the guide vanes, using different solidification states, would also have a positive influence on the economic efficiency.

The broad spectrum of alloying elements constitutes a great challenge for welding technology. In particular, the weldability of the age-hardening nickel-base alloy is correlated with the aluminium and titanium content [6]. To increase strength, aluminium and titanium are withdrawn from the γ -matrix after solution heat treatment during the ageing process and a γ' phase $\text{Ni}_3(\text{Al}, \text{Ti})$ is precipitated. This decreases the lattice parameter and increases the lattice distortion. The heat treatment is usually carried out after the welding process. Welding after heat treatment would soften the material in the area of the weld seam and the HAZ. However, the strengthening measure after the welding process can lead to crack formation. Due to the lower aging temperature range compared to the solution annealing temperature, aging processes already occur during the heating phase to solution annealing temperature and thus γ' precipitation. A superposition of the stresses resulting from the lattice distortion processes and the residual welding stresses in the HAZ that have not yet been removed can lead to the maximum material yield strength being exceeded and to failure of the component [7]. For this reason the residual welding stress should be reduced to a minimum.

Furthermore, hot cracking is to be considered as critical, especially during welding. When welding nickel-base alloys, a differentiation is essentially made between two types of hot cracking. Intercrystalline liquation cracks in the HAZ, according to the mechanism of constitutional liquefaction of the low-melting phases, as well as solidification cracks in the seam. For both crack types, crack initiation is due to thermally induced stresses. Cracks in the weld metal occur mainly during solidification. Due to the different solubility of the alloying elements in the melt, the concentration changes continuously in the solidification interval. The degree of segregation depends on the solidification rate. This is generally influenced by the welding speed during welding. In addition, the solidification rate changes with the temperature gradient G at each location of the weld pool isotherms. Both the weld pool shape and the microstructure are determined by these two values. During the solidification interval, the solidification type changes continuously from planar to equiaxial dendritic [7, 8]. Solidification starts in the area of the highest cooling rate or the highest temperature gradient at the solidification edge to the base material. The crystals grow perpendicular to the solidification isotherms. With increasing welding speed, the weld pool shape changes from elliptical to drop-shaped with crystal growth almost perpendicular to the welding direction. The segregation front proceeds in the remaining melt with the interdendritic distance unfavourable to the shrinkage stresses resulting from the process. The consequence is crack initiation in the melt.

With the electron beam, a precise and versatile tool is available. On the one hand, critical residual welding stresses can be reduced by specific heat control and on the other hand, the solidification morphology can be positively influenced. The welding process thus offers the ideal conditions for improving the seam quality in terms of crack reduction when welding Alloy 247 LC. The welding speed is investigated as a primary parameter of the process for modifying the heat control.

2 Experimental Setup

2.1 Material

For the investigations, the precipitation-hardening nickel-based alloy Alloy-247 LC was examined in the conventionally cast (CC) state and later also in the directionally solidified state. After the casting process, the material was solution annealed at 1232 °C for 2 h 15 min under reduced atmospheric pressure. Subsequently, the specimens for the welding tests were eroded out of the ingots and milled to final dimension (100 × 60 × 6). Both the CC and the DS base material have a coarse-grained structure with macroscopic dendrite spacing. In the interdendritic areas of the base material a multi-phase structure with γ' precipitations of Ni₃(Al,Ti) in the γ matrix is present. The size and shape of the γ' precipitates is inhomogeneously distributed due to the missing aging process after the solution heat treatment. This chemical composition is presented in Table 1.

Table 1. Composition of Alloy-247 LC (wt. %). Examined with atomic emission spectroscopy

	Ni	C	Si	Cr	Co	Mo	W	Ti	Al	Ta	Hf	Fe
Alloy-247 LC	bal.	0.07	0.1	8.2	9.0	0.5	8.9	0.8	5.6	3.5	1.6	0.4

2.2 Process

The electron beam welding machine ProBeam K-7 with 120 kV acceleration voltage was used as a test facility. The welding was performed at a pressure of 10^{-4} mbar and with a working distance of 400 mm to the focus lens. The focus position was left on the component surface at all beam currents. As in practice a certain welding depth is required, all tests were welded with a constant welding depth of 5 mm ± 0.5 mm. This also provides comparability of the results. For this purpose, a power required for the welding depth was determined for each welding speed. An overview of the parameters investigated is shown in Table 2. It can be seen that with decreasing welding speed a higher energy per unit length is required to achieve the same weld depths. Before welding, the plates were cleaned in an acetone ultrasonic bath for 10 min and then clamped with a vice perpendicular to the welding direction, over the entire length. A 90 mm long seam was welded in the middle of the 100 mm long sample.

Table 2. Overview of the examined parameters

Alloy-247 LC		Specimen thickness [mm]	E [J/mm]	U _b [kV]	I _b [mA]	V _s [mm/s]	Focus position
CC	BoP	6.0	960	120	4.0	0.5	surface
CC	BoP	6.0	600	120	5.0	1.0	surface
CC	BoP	6.0	450	120	7.5	2.0	surface
CC	BoP	6.0	270	120	9.0	4.0	surface
CC	BoP	6.0	210	120	10.5	6.0	surface
CC	BoP	6.0	164	120	10.9	8.0	surface
CC	BoP	6.0	138	120	11.5	10.0	surface
CC + DS	tack welding	12.0	78	120	6.5	10.0	surface
CC + DS	joint welding	12.0	1680	120	14	1.0	surface

2.3 Evaluation Methods

In order to be able to evaluate the welding results and create a sufficient basis for interpretation, both metallographic and radiographic examinations were carried out. For this purpose, all samples were cut out of the seam according to Fig. 1. The first and last 5 mm of the seam were not considered in the evaluation.

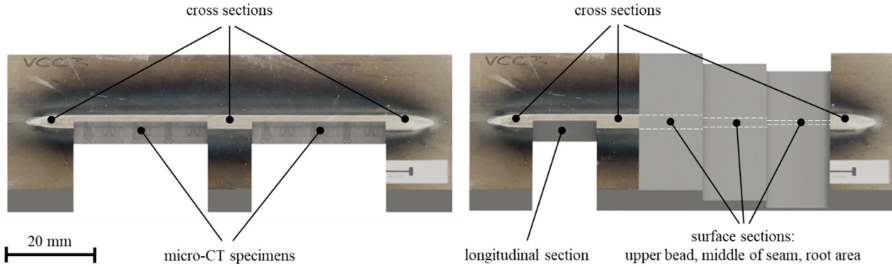


Fig. 1. Drawing of the mechanical sample preparation for three transverse sections and two micro-CT images (left) and of the sections for the dendrite investigation (right)

In the first step, all samples were examined for surface cracks with the scanning electron microscope. The crack position and the total crack length were determined. These results are used as a first indication for crack evaluation. The crack identification and localization inside the weld was performed with the assistance of microCT scans. For this purpose, samples of the same size were taken from the weld samples. Due to the high density of the material, the sample geometry was limited to a maximum thickness of 3.3 mm. One side was milled to the centre of the seam and subsequently the 3.3 mm thick sample was cut out. A total of 2 specimens per examined parameter were prepared for the Micro CT examination. The crack positions and crack lengths were also determined. Due to the lack of information about the types of crack, metallographic

examinations of transverse, longitudinal and surface sections were carried out in addition to the microCT. For this purpose the samples were etched according to Kalling-II (100 mL ethanol, 100 mL hydrochloric acid (32%) and 5 g copper(II)-chloride) at 21 °C for 45 s and then magnified with a microscope. Simultaneously to crack identification, the secondary dendrite arm spacing (SDAS) was measured using the metallographically prepared samples according to [9]. Due to the continuously changing welding isotherm and the associated dependence of the dendrite growth direction, the sample preparation for the determination of the primary dendrite spacing is very complex. In addition, the direction of dendrite growth changes with the welding speed and thus the effort for an adequate measurement. For this reason, the dendrite spacing was not measured within the scope of this work.

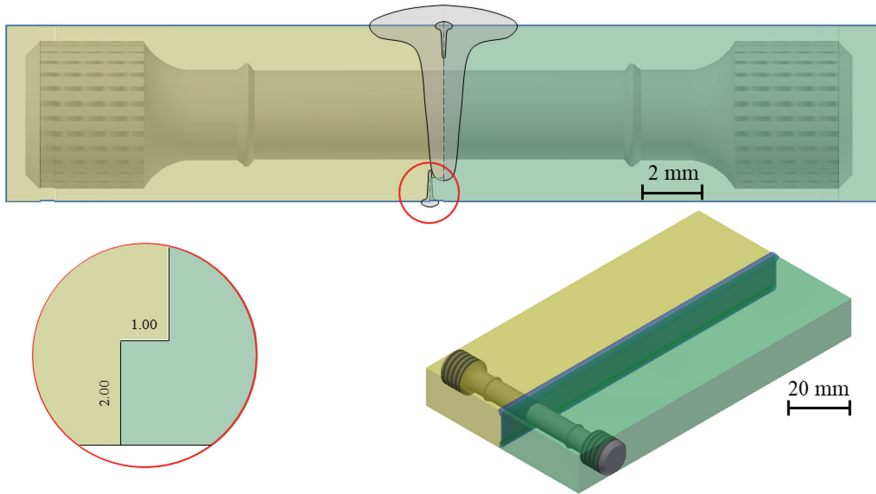


Fig. 2. Drawing of the welding preparation and the position of the creep specimen

Furthermore, specimens for creep tests were welded with the crack-reduced 1.0 mm/s parameter. For this purpose, the parameter for a 12 mm thick joint weld (Alloy-247 CC to Alloy-247 DS) was adjusted, Table 2. Due to the low viscosity of the melt and the resulting unacceptable weld sinkage welding in PA-position, the specimen preparation was selected according to Fig. 2. Like the preliminary tests before, the specimens were heat-treated, mechanically prepared and then cleaned with acetone. Before the joint welding, the samples were tack welded on both sides by an 80 mm long linear seam. The parameters are shown in Table 2. By choosing a narrow tack weld geometry, the subsequent weld ensures that the cracked tack weld is completely over-welded in the welding area.

The samples for the creep tests were extracted according to Fig. 2. A total of 10 creep specimens were prepared from two joint welds. Subsequently, the samples were subjected to a three-stage heat treatment. Solution annealed at 1243 °C for 4h, in the stabilization annealed at 1080 °C for 2 h and ageing at 870 °C for 20 h.

3 Results

3.1 Influence of the Welding Speed on the Welding Depth

The weld geometry has a significant influence on the heat distribution over the welding depth and thus on the stress distribution in the component. Figure 3 shows the seam geometries in relation of the welding speed. At welding speeds of 1 mm/s and 2 mm/s it can be seen that the weld depth of 5 mm \pm 0.5 mm is not achieved. Due to the low welding speed, the leading heat flow changes continuously the welding depth over the entire weld seam length. In addition, nail head formation increases and the ratio of weld depth to weld width decreases significantly. Due to the low thermal conductivity of the alloy, this effect can be observed up to a welding speed of 4 mm/s.

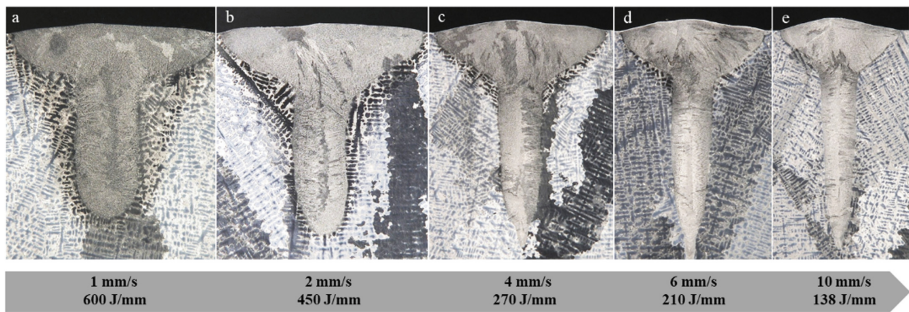


Fig. 3. Light microscopy images of cross-sections at different welding speeds

3.2 Influence of the Welding Speed on the Dendrite Morphology

The welding speed as a direct parameter has a significant influence on the temperature gradient G and the crystallization rate R . Figure 4 illustrates the influence of the welding speed on SDAS. The SDAS decreases with increasing welding speed due to the high solidification rate. Furthermore, the SDAS is inhomogeneous over the seam depth. Towards lower welding speeds, the SDAS increases in areas of the pronounced nail head. Regardless of the welding speed, the solidification rate is highest in the root zone. As a result, the dendrite arm distance in the root area is closer than in the other areas of the weld.

Furthermore, the inhomogeneity of the SDAS increases over the seam depth to higher welding speeds. At 1.0 mm/s welding speed, the SDAS varies over the seam depth by only 1.2% of the maximum value. In contrast, the variation at higher welding speeds

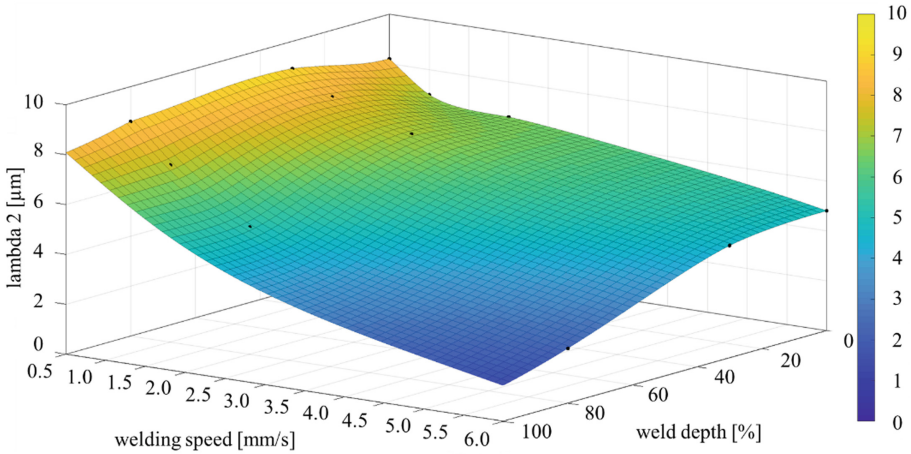


Fig. 4. Dendrite arm distance over the welding depth in percent depending on the welding speed. Evaluated by means of transverse, longitudinal and surface sections in three areas of the seam (upper bead, seam centre and seam root).

(6.0 mm/s) increases to approximately 50% of the maximum value. According to Whitesell [10], the SDAS is dependent on both the temperature gradient and the solidification rate. In welding, however, these two indirect parameters cannot be separated from the welding speed. The solidification rate is inevitably dependent on the temperature gradient. This allows a conclusion to be drawn about the qualitative course of the temperature gradient.

3.3 Crack Formation Depending on the Welding Speed

The first evaluation of a weld seam is always performed visually on the surface. The result gives a first indication of the seam quality. Figure 5 shows an example of three SEM images of seam surfaces that were welded with different speeds. The energy per unit length was kept constant at 100 J/mm.

It can be seen that the crack length increases with increasing welding speed. In addition, the crack position shifts from the base material in the direction of the weld seam. At high welding speeds, the crack progresses along the solidification line perpendicular to the welding isotherm. In this area, thermal stresses occur perpendicular to the dendrite growth direction and tear open the still liquid interdendritic area. With decreasing welding speed, more time is available for solidification. On the one hand, microcracks can be filled due to the larger dendrite spacing and the subsequent melt flow, on the other hand, the thermal stress (transverse to the welding direction) only develops when the critical area (which runs transverse to the stress) has sufficient strength. According to Rappaz [11], the hot crack tendency decreases with higher SDAS and lower thermal stress. However, the residual stress states in Fig. 5 cannot be compared due to the different stiffness states. An investigation with constant welding depth minimizes the possible influence of stiffness to a minimum. Figure 6 shows the total crack length on the upper

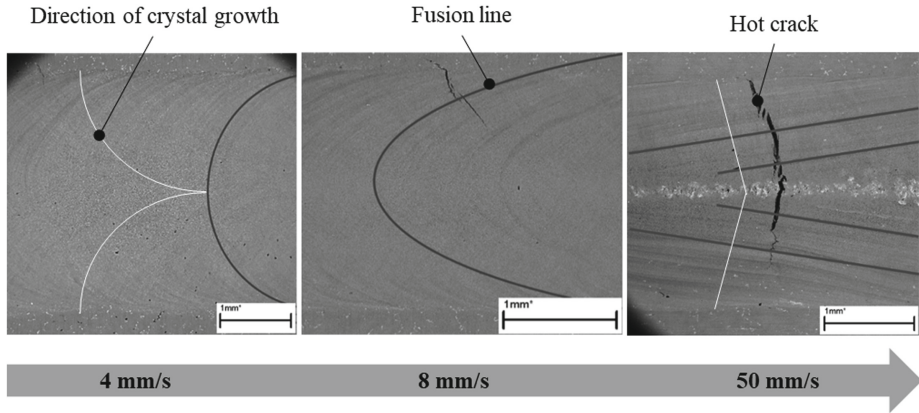


Fig. 5. SEM Images of weld pool geometry, dendrite growth direction and crack initiation direction depending on the welding speed

bead over the welding speed at constant welding depth. For this purpose all cracks were cumulated to a total crack length.

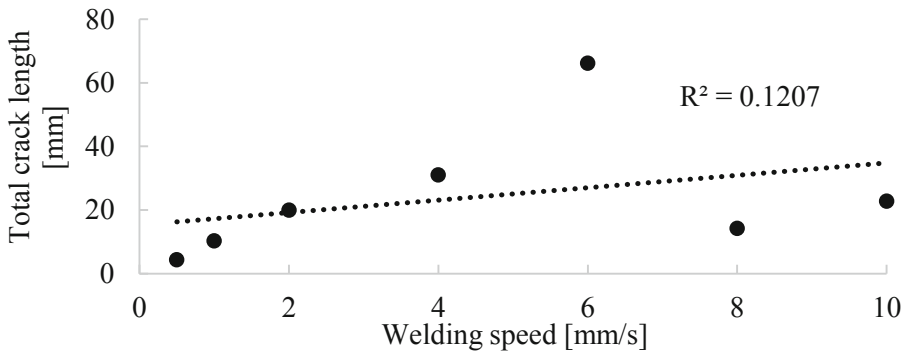


Fig. 6. Correlation between welding speed and total crack length on the upper bead at constant welding depth. Evaluated on SEM images.

The total crack length increases with increasing welding speed. At higher speeds, the maximum crack length is limited by the seam width and thus the total crack length on the upper bead does not increase significantly. In addition, a differentiation is made in the following between two types of hot cracking. At higher welding speeds, the solidification crack mainly occurs in the seam. Where, on the other hand, the liquation cracks occurs in the HAZ at lower welding speeds. In the range between 2 mm/s and 8 mm/s welding speed, both types of hot crack are observed. For this reason, a maximum of the total crack length at 6 mm/s welding speed is shown in Fig. 6.

A microCT evaluation of the weld seams in Fig. 7 shows a similar correlation between the welding speed and the total crack length.

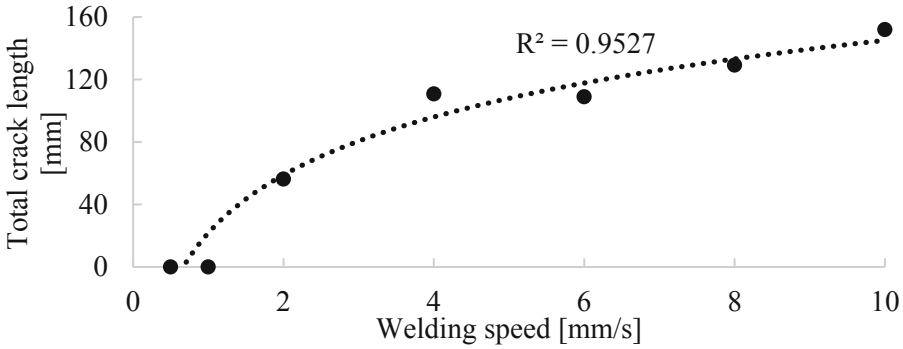


Fig. 7. Correlation between welding speed and total crack length in the seam at constant welding depth. Evaluated on microCT images.

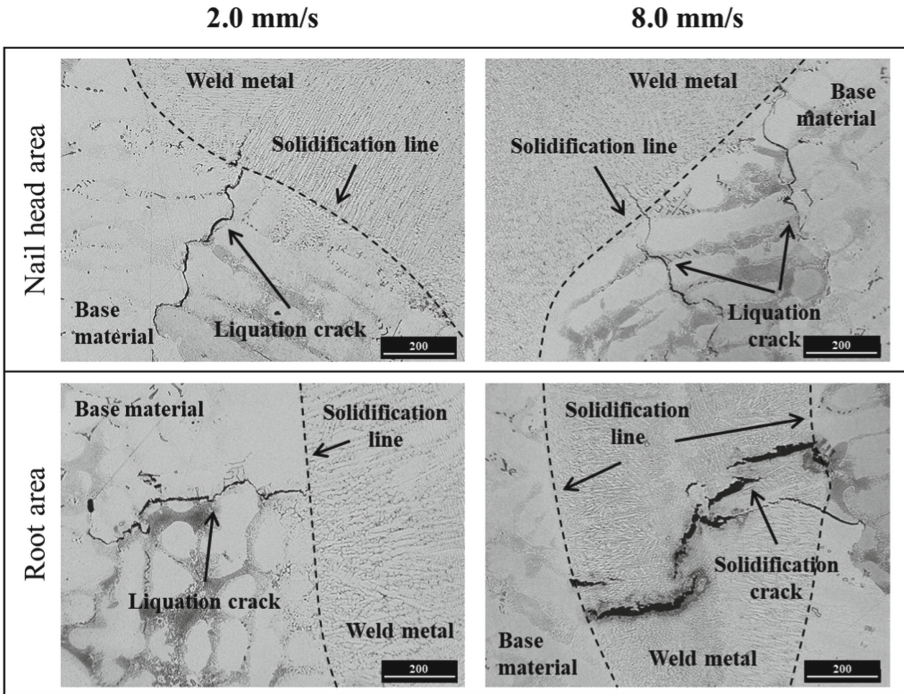


Fig. 8. Light microscopy images showing a parameter and position dependent crack formation near the nail head and in the root area of a weld for 2.0 mm/s and 8.0 mm/s welding speed

In contrast to the evaluation of the upper bead, the total crack length in the weld seam increases linearly with increasing welding speed. A metallographic examination was carried out to identify the types of cracks. Figure 8 shows an example of the typical hot cracks when welding Alloy-247 LC. Comparable to the crack investigations on the upper bead, only predominantly hot cracks occur in the HAZ at lower welding speeds.

In contrast, at higher welding speeds the solidification crack in the deep welding area cannot be avoided. According to Fig. 4, a higher temperature gradient can be assumed due to the smaller dendrite arm distance in this area. This in turn has a negative effect on the thermally induced residual stresses and the solidification rate, which are mainly responsible for the solidification cracks in the weld metal.

3.4 Welding of Creep Specimens

The previous results indicate that at lower welding speeds, the total crack length decreases to a minimum when welding Alloy-247 LC in the CC and solution heat treated condition. A weld joint between a CC and a DS (transverse to the direction of weld) specimen was investigated in the following. Heat treatment subsequent to the welding process increases the γ' precipitation and thus the creep resistance to higher temperatures. For this purpose, the samples were solution annealed at 1243 °C for 4 h after welding, stabilised at 1080 °C for 2 h and aged at 870 °C for 20 h.

For the creep tests the 1.0 mm/s welding speed parameter was preferred to the 0.5 mm/s parameter due to the lower leading heat flow. The beam current was adjusted to the sheet thickness. Despite clamping perpendicular to the welding direction, the specimens were tack welded with a welding depth of 2.1 mm on both sides over a length of 80 mm. The creep test specimens were mechanically prepared as shown in Fig. 2. The results of the creep test thus reflect the weld quality in the middle area of the weld.

Figure 9 shows the results of the creep tests of welded and aged specimens, at a test temperature of 850 °C and 950 °C in comparison with the base materials. The individual measuring points of the welded specimens are on the extrapolated minimum curve of the CC base material.

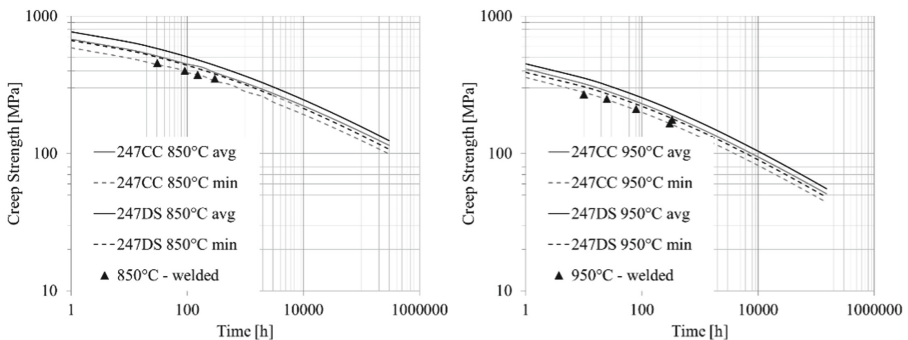


Fig. 9. Creep rupture strengths of the hybrid weld (CC with DS) at two different test temperatures (850 °C and 950 °C). Mean strength of the base materials (solid lines) and the specified minima according to Siemens (dashed lines).

This shows that the liquation cracks occurring parallel to the direction of the load or the cracks that could occur during post-heat treatment have no significant influence on the creep strength.

4 Conclusion

In this study it could be shown that the hot cracking tendency could be reduced with a reduced temperature gradient. As a direct parameter in electron beam welding, the welding speed has a significant influence on the temperature gradient and thus on the solidification rate and weld pool geometry while the power density distribution of the beam remains constant. At lower welding speeds the solidification crack in the seam and on the upper bead could be completely suppressed due to the lower temperature gradient. As Rappaz [11] has already shown with the hot cracking criterion, the SDAS and the temperature gradient correlate with the hot cracking probability (solidification crack). In contrast, the liquation crack in the HAZ could not be suppressed either in the area of the nail head or in the area of the deep welding. However, at lower welding speeds, the total length decreased significantly. Furthermore, creep tests have shown that possible liquation cracks in the area of the deep welding area that occurring parallel to the direction of the load (transverse to the welding direction) have no influence on the high-temperature strength. Even a heat treatment to increase strength after the welding process has no negative influence on crack formation with the optimized welding parameter.

References

1. Mom, A.J.A.: Introduction to Gas Turbines. Woodhead Publishing, Sawston (2013). <https://doi.org/10.1533/9780857096067.1.3>
2. Betteridge, W., Shaw, S.W.K.: Development of superalloys. *Mater. Sci. Technol.* **3**(9), 682–694 (1987)
3. Sims, C. T.: A history of superalloy metallurgy for superalloy metallurgists. *Superalloys 1984*. The Metallurgical Society of AIME, Warandale (1984)
4. Harris, K., Erickson, G.L., Schwer, R.E.: Directionally solidified and single-crystal superalloys, properties and selection: irons, steels, and high-performance alloys. *ASM Handbook Committee* (1990)
5. Harris, K., Erickson, G.L., Schwer, R.E.: MAR M 247 derivations - CM 247 LC DS alloy and CMSX single crystal alloys: properties & performance. *Superalloys 1984*. The Metallurgical Society of AIME, Warandale (1984)
6. Kelly, T. J.: Welding metallurgy of investment cast nickel-based superalloys. *Weldability of Materials*, pp. 151–157. ASM International, Materials Park, OH (1990)
7. Kou, S.: *Welding Metallurgy*, 2nd edn. Wiley, New Jersey (2003)
8. Schulze, G.: *Die Metallurgie des Schweißens – Eisenwerkstoffe - Nichteisenmetallische Werkstoffe*, 4th edn. Springer, Berlin (2010)
9. BDG-Richtlinie VDG-Merkblatt: Bestimmung des Dendritenarmabstandes für Gussstücke aus Aluminium-Gusslegierungen, P220, BDG-Informationszentrum Giesserei, Düsseldorf (2011)
10. Whitesell, H.S., Li, L., Overfelt, R.A.: Influence of solidification variables on the dendrite arm spacings of ni-based superalloys. *Metall. Mater. Trans. B.* **31B**, 546–551 (2000)
11. Rappaz, M., Drezet, J.-M., Gremaud, M.: A new hot-tearing criterion. *Metall. Mater. Trans. A.* **30A**, 449–455 (1999)